PROCEEDINGS OF SCIENCE

Newly Discovered Low Energy Resonances In The ^{22}Ne(p,γ)^{23}Na At LUNA

Federico Ferraro[*†]
Università degli Studi di Genova and INFN, Sezione di Genova
E-mail: federico.ferraro@ge.infn.it

The neon-sodium cycle of hydrogen burning influences the synthesis of the elements between ^{20}Ne and ^{27}Al in red giant stars, asymptotic giant stars, and novae explosions. In order to reproduce the observed elemental abundances, the cross sections of the reactions involved in the nucleosynthesis process should be accurately known. The ^{22}Ne(p,γ)^{23}Na reaction rate is very uncertain because of a large number of unobserved resonances lying in the Gamow window. A new direct study of ^{22}Ne(p,γ)^{23}Na has been performed at the Laboratory for Underground Nuclear Astrophysics (LUNA) in Gran Sasso using a windowless gas target and two different experimental setups. Three resonances (156.2, 189.5, and 259.7 keV) have been observed for the first time in a direct experiment, using two high-purity germanium detectors. Further investigations have been devoted to the tentative resonances at 71 and 105 keV, using a six-fold, optically segmented BGO detector surrounding the interaction volume. The resulting reaction rate is significantly different from the STARLIB 2013 evaluation at temperatures around 0.1 GK, relevant to nucleosynthesis in asymptotic giant branch stars.

The 26th International Nuclear Physics Conference
11-16 September, 2016
Adelaide, Australia

[*]Speaker.
[†]On behalf of the LUNA collaboration.

© Copyright owned by the author(s) under the terms of the Creative Commons Attribution-NonCommercial-NoDerivatives 4.0 International License (CC BY-NC-ND 4.0).

PoS(INPC2016)148

1. Introduction

The oxygen-sodium anticorrelation in globular clusters [1] requires, in order to be understood, a precise knowledge of the sodium production and destruction rates. One common explanation is that the stars showing this anticorrelation were formed in an environment that was polluted by previous generation AGB stars. Indeed the AGB stars may reach, at the base of their convective H-rich envelope, temperatures high enough to let the Hot Bottom Burning occur and change the surface abundances thanks to convection.

It has been found, for metal-poor and very metal-poor AGB stars, that models would better match the observations if ^{22}Ne$(p,\gamma)^{23}$Na reaction rate was higher than the literature one [2]. Another possible explanation has been proposed in [3], suggesting a core hydrogen burning and rotation-driven winds.
In both cases ^{23}Na is produced via the ^{22}Ne$(p,\gamma)^{23}$Na reaction, which is part of the neon-sodium cycle of hydrogen burning. The ^{22}Ne$(p,\gamma)^{23}$Na reaction cross section is required in order to calculate the reaction rate. A new experimental effort was asked [6] in order to reduce the uncertainties

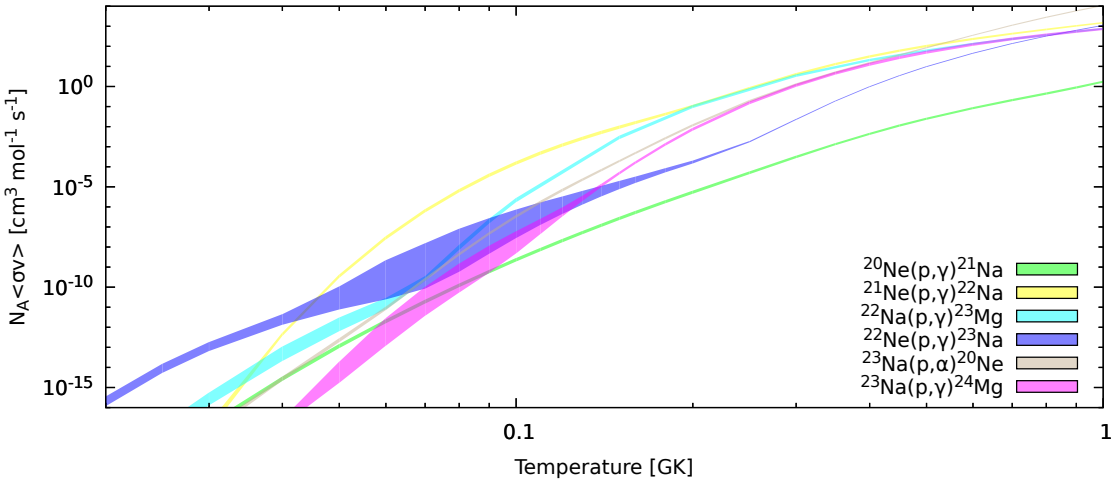

Figure 1: TNRR of the different reactions involved in the NeNa cycle. ^{22}Na(p,γ)^{23}Mg reaction rate is from [4]. ^{22}Ne(p,γ)^{23}Na reaction rate is from [5].

on the cross section, thus reducing the uncertainty on the reaction rate and the predicted ^{23}Na abundance.

Many resonances contribute to the ^{22}Ne$(p,\gamma)^{23}$Na cross section. The resonances above 400 keV, which affect the thermonuclear reaction rate for temperatures $T > 0.5$ GK, have already been studied [7, 8, 11, 12]. Below 400 keV only a few resonance strengths have been directly measured so far, yet many upper limits have been put [13, 5, 8]. Some indirect measurements have been carried out [23, 14, 24], but they rely on spin-parity assignments or spectroscopic factor normalizations which were uncertain. Consequently, the very existence of the resonances at E_p^{res} = 71, 105 and 215 keV is considered as tentative [23, 14, 13].

The way experimental upper limits and indirect data have been considered in the literature led to different reaction rate evaluations. The reaction rate has been calculated in 1999 by the NACRE

PoS(INPC2016)148

collaboration [25] from the resonance measurements [8, 9] and the direct capture component [9]. Later on, a similar evaluation has been performed in 2001 [14], updated in 2010 [10, 11] and again in 2013 [4] by the STARLIB group, completely disregarding the uncertain resonances. As a result, the NACRE and the STARLIB compilations differ up to a factor of 1000. LUNA recently investigated the low-energy resonances in the ^{22}Ne(p,γ)^{23}Na reaction and gave a new estimation of the reaction rate. Shortly after, a new measurement by LENA [15] was carried on, as well as a new evaluation of the reaction rate.

1.1 LUNA

LUNA (Laboratory for Underground Nuclear Astrophysics) is located in the Gran Sasso National Laboratory (LNGS), Italy. To date, LUNA operates the world's only deep underground accelerator in running conditions. The accelerator consists of a 400 kV electrostatic accelerator providing high currents with very small energy spread and good long-term stability [16, 17]. LUNA benefits from a 1400 m thick rock overburden ($\approx$ 3800 m.w.e.), which reduces the cosmic rays induced background by a factor of 10^6 and 10^3 for what concerns the muon component and the neutron component respectively [26, 27] leading to extremely low cosmic background.

LUNA recently studied the ^{22}Ne$(p,\gamma)^{23}$Na reaction using two different setups. During the first phase of the experiment, two high-purity germanium (HPGe) detectors were used [13, 5]. This phase was devoted to the measurement of the resonances above 150 keV (in the laboratory system). In a second phase of the experiment, an optically segmented Bismuth Germanate (BGO) detector with large solid angle coverage [18] was used to investigate on the resonances at 71 and 105 keV and to measure the non-resonant component of the cross section. A description of the experiment will be briefly presented.

2. Experimental setup

A windowless extended gas target was used in this experiment. Three pumping stages realize a strong pressure gradient between the interaction chamber and the beamline (figure 2).

A replica of the interaction chamber was provided with side flanges and tubes to measure pressure and temperature of the target gas and determine its density all along the beam path. Capacitance pressure gauges were used to measure the pressure in different positions all along the target chamber. A feedback system always measured the nominal reference pressure in the middle of the interaction chamber and acted on the gas inlet to keep the pressure stable. The pressure profile was measured for different nominal pressures. ^{22}Ne pressure profiles were measured in steps of 0.5 mbar from 0.5 mbar up to 4 mbar. Temperature profiles were measured inside the target chamber using four Pt100 RTDs reaching the beam path.

Using measured pressure and temperature data, the gas density was calculated using the ideal gas law

$$\frac{N}{V} = \frac{P}{k_B T} \tag{2.1}$$

where the term on the left is the gas density and k_B is the Boltzmann constant.

The gas target does not allow for an electrical measurement of the beam current, thus a power compensation calorimeter is used for a real time measurement [28]. The beam stop can be heated

PoS(INPC2016)148

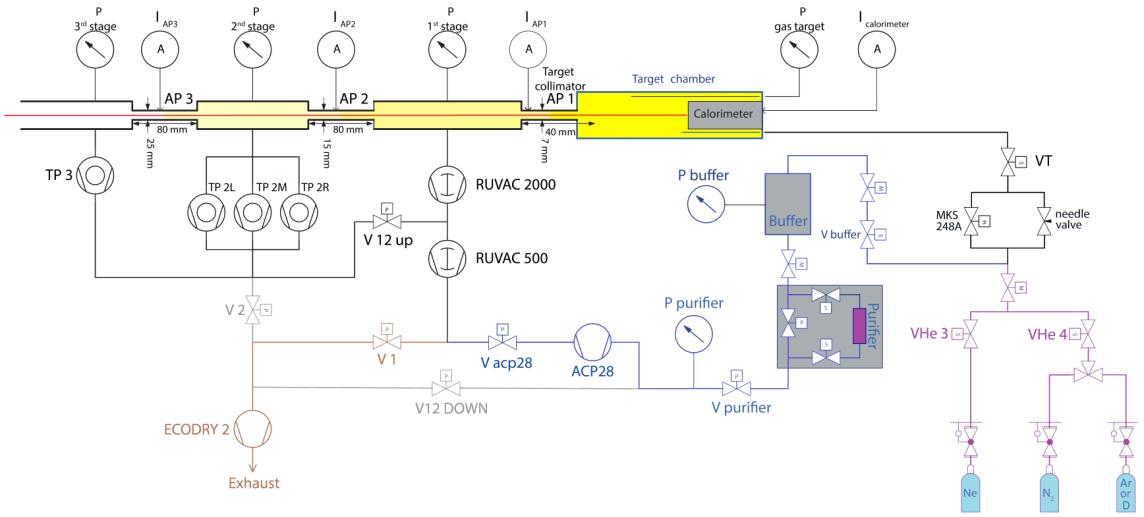

Figure 2: Differential pumping system schematic. The beam comes from the accelerator on the left, passes through the apertures AP3, AP2 and AP1, enters the target chamber and stops on the calorimeter.

up either by resistors or the beam, thus the more power is provided by the beam, the less is provided by resistors. If W_0 is the power delivered by resistors while the beam is off and W_{run} is the power delivered when the beam is on, the calorimetric beam power is $W_{cal.} = W_0 - W_{run}$. The current is given by

$$I = \frac{W_{cal.}}{\left(E_p - \Delta E_p^{target}\right)} e \tag{2.2}$$

where E_p is the beam energy as it comes out of the accelerator and ΔE_p^{target} is the energy the beam loses passing through the target gas. Since the energy loss depends on the beam current itself, a beam-heating correction has to be applied [19], depending on the gas pressure and the beam current. The beam-heating correction in neon was studied in [20] using a collimated sodium iodide (NaI) detector and the resonance scan technique. To reduce the systematic uncertainty associated to the beam current measurement, a calibration was performed against the electrical measurement in vacuum.

2.1 HPGe setup

The HPGe detectors, of 90% and 135% relative efficiency, were collimated at 90° and 55° with respect to the beam direction. A 22-30 cm thick copper and lead shield was built around the detectors to prevent the background caused by environmental radioactive isotopes. The whole shielding was enclosed in a box and flushed with nitrogen.

Two independent acquisition chains were used, one of which provided list-mode data. The efficiency was measured along the beam direction by means of radioactive point-like sources (^{7}Be, ^{137}Cs, ^{60}Co and ^{88}Y) and the well known ^{14}N$(p,\gamma)^{15}$O resonance at E_p^{res} = 278 keV, populated in different positions inside the chamber. Due to the close geometry, the summing-out correction was determined thanks to a GEANT simulation.

PoS(INPC2016)148

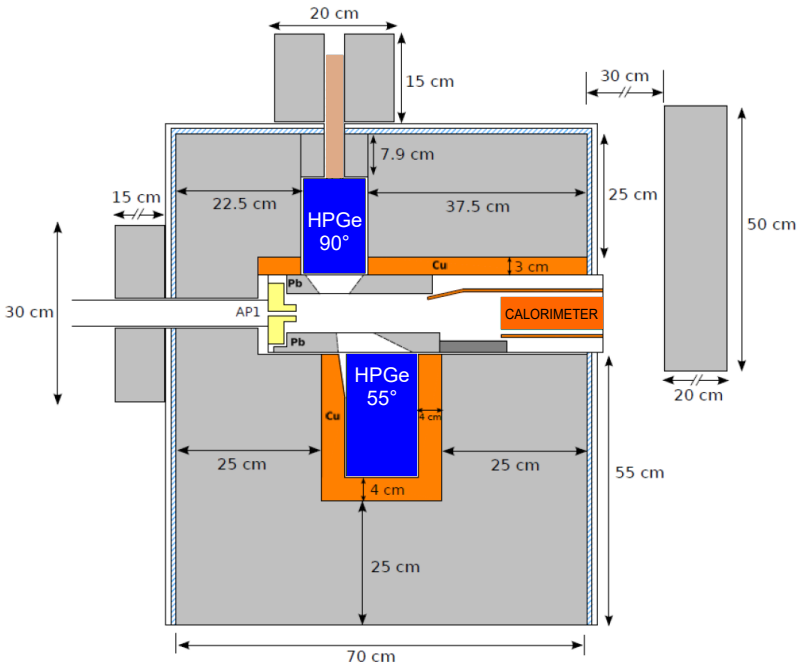

(a) Sketch of the HPGe setup.

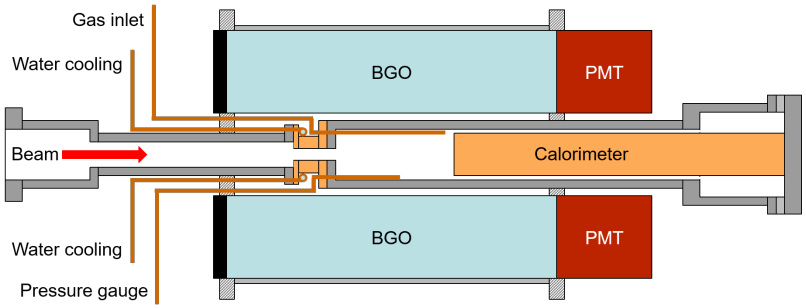

(b) Sketch of the BGO setup.

Figure 3: Drawings of the experimental setups used in the study of the ^{22}Ne$(p,\gamma)^{23}$Na reaction at LUNA.

2.2 BGO setup

The BGO detector is composed by six scintillating crystals arranged in a hexagonal configuration to surround the interaction volume. The crystals, 28 cm long and 7 cm thick at the thinnest point, are housed inside a steel casing provided with a 6 cm borehole. Signals coming from the six anodes are independently amplified and digitized. Data from each channel were initially saved in binary files and then collected into `ROOT` files for each run. For each acquired event the timestamp were the energy are saved.

Once the linearity of the calibrations was verified using ^{14}N(p, γ)^{15}O peaks, each spectrum was calibrated by an automated routine, using three of the low energy peaks originating from nat-

PoS(INPC2016)148

ural background: 1460 keV peak from ^{40}K, 2204 keV peak from ^{214}Bi and 2614 keV peak from ^{208}Tl. Since all events are stored with their timestamp and energy, it is possible to recover coincidence information and perform coincidence analysis. Events acquired in a 3.5 μs wide window are grouped together and the sum of their energies is recorded in the addback spectrum.

^{7}Be, ^{137}Cs, ^{60}Co and ^{88}Y radioactive point-like sources were used to measure the detector efficiency at different energies in several positions along the beam axis inside the interaction chamber. Because of the particular geometry and the high detection efficiency of the BGO detector, a new simulation was developed to determine the efficiency. The simulation was tuned to match sources data as well as the spectrum originating from the ^{14}N$(p,\gamma)^{15}$O resonance at $E_p^{res} = 278$ keV. Good agreement was obtained between simulations and data both for single segments and addback spectra.

3. Measurements

3.1 HPGe phase

The high resolution of the HPGe detectors allows to clearly distinguish the peaks originating from the ^{22}Ne$(p,\gamma)^{23}$Na reaction. For each resonance a scan was performed, changing the beam energy in steps of 1-2 keV and monitoring the yield of the $E_\gamma = 440$ keV peak, which is related to the transition from the first excited state to the ground state and is expected to be largely populated in ^{23}Na decay. Then, a long measurement on top of the yield curve was performed for the observed resonances.

Thanks to the underground location, spectra were extremely clean above 2.6 MeV. The lead shielding provided an effective reduction of the natural background below 2.6 MeV as well, and the high resolution allows for a rather simple identification of the peaks and background subtraction. A portion of the spectrum of the $E_R = 259.7$ keV resonance is shown in figure 4. The background was

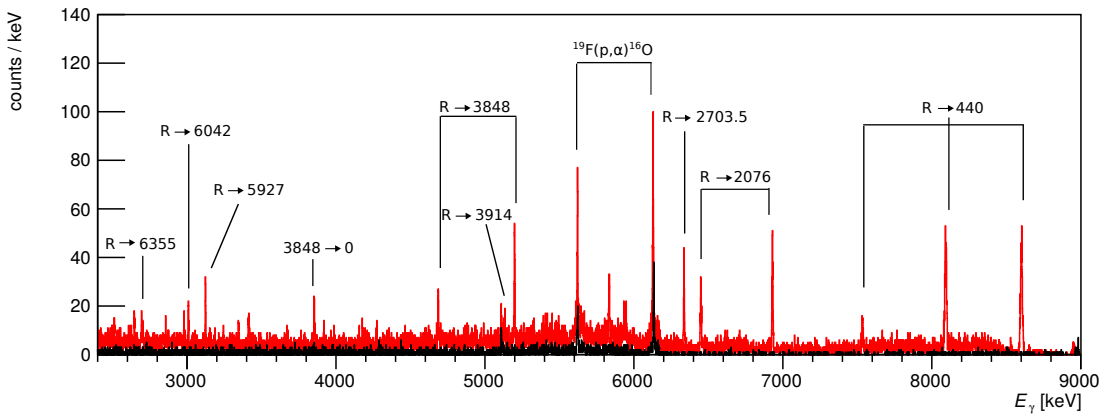

Figure 4: Portion of the spectrum of the $E_R = 259.7$ keV resonance as seen by the detector at 55°.

subtracted considering the interpolation from regions on both sides of the peaks. Branching ratios were determined using the detector at 55°, taking into account the detection efficiency corresponding to each peak. Updated resonance energies were determined as well, taking into account the uncertainty on the energy loss in the target gas and the systematic uncertainty on the beam energy.

PoS(INPC2016)148

The resonance strengths were calculated, assuming an infinitely thick target and a negligible resonance width, through the following relation:

$$\omega\gamma = \varepsilon_r \frac{Y_{max}}{\lambda_R^2/2} \frac{m_t}{m_t + m_p} \tag{3.1}$$

where ε_R and λ_R are the stopping power and the De Broglie wavelength at the resonance energy and m_p and m_t are the masses of the projectile and the target. The maximum yield was obtained considering all of the observed primary transitions and their detection probability:

$$Y_{max} = \frac{1}{Q} \sum_i \left(\frac{N_i}{\eta_i} \right) \tag{3.2}$$

where N_i is the number of detected events measured for the primary transition i and η_i is the associated detection efficiency.

A detailed description of the measurements is given in [5]. The results on the investigated resonances are shown in table 1.

3.2 BGO phase

The BGO detector, thanks to its high efficiency and the large solid angle coverage, is able to effectively detect the multiple γ-rays originating from the decay of the excited state of the final nucleus, causing a peak at $Q + E_p^{cm}$ to arise in the addback spectrum.

Background subtraction was more complicated in the analysis of the BGO phase data. Below 3 MeV natural background dominates the spectra. Several γ-rays originate from ^{214}Bi, ^{208}Tl and ^{40}K [21], increasing the counts at low energy.

Above 3 MeV cosmic rays induced background usually plays a critical role in surface laboratories, where the reaction signal is often overwhelmed by the background. In this region the beam induced background (BIB) represents the biggest impediment to the measurement, especially using a high-efficiency setup with low energy resolution. Nuclear reactions involving light contaminants produce high energy gamma rays, leading to a background which depends on the contaminants in the setup, their position and the beam energy [22]. To take the BIB into account and subtract it from the reaction spectra, blank spectra with an Ar target were acquired.

Equation 3.1 was used to calculate the resonance strength, using

$$Y_{max} = \frac{N_{sum}}{Q\eta_{sum}} \tag{3.3}$$

where N_{sum} is the number of events in the peak at $Q + E_p^{cm}$ and η_{sum} is the detection efficiency for the selected region of interest. η_{sum} depends on the decay scheme of the final nucleus and is evaluated by the simulation using the branching ratios measured during the HPGe phase.

After the measurements on the resonances at 156.2, 189.5 and 259.7 keV, the BGO detector was devoted to the investigation on the tentative resonances at 71 and 105 keV. The non-resonant component of the cross section was measured as well at four different energies. The analysis of the BGO data is still ongoing.

PoS(INPC2016)148

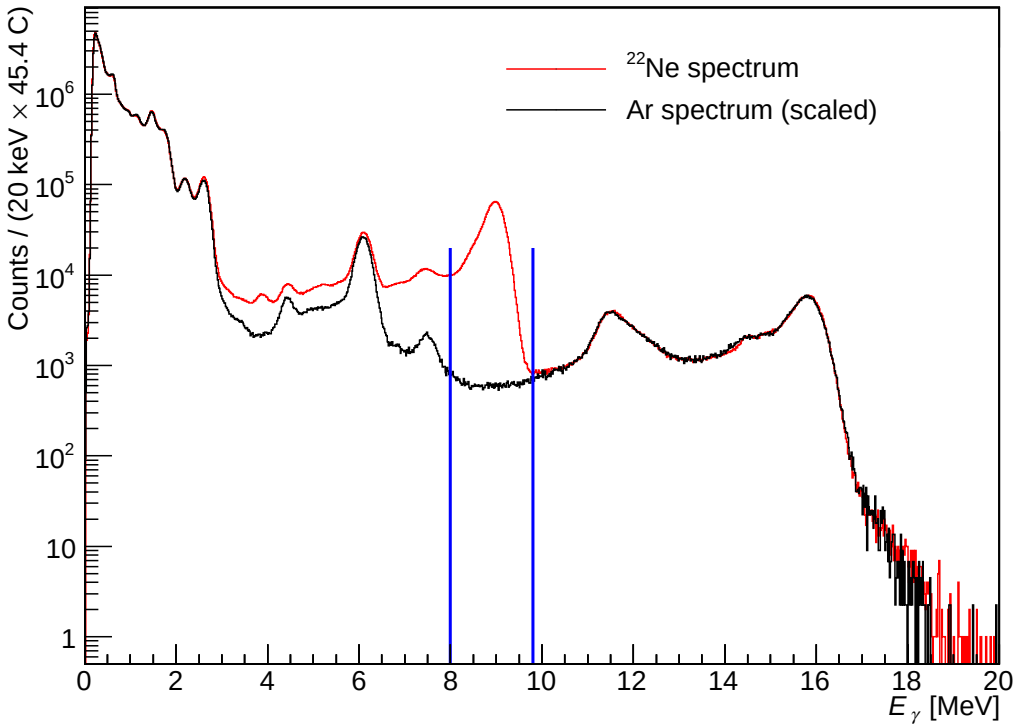

Figure 5: Addback spectra for the resonance at $E_R = 259.7$ keV. The red spectrum was acquired with a ^{22}Ne target, while the black spectrum was acquired with an Ar target. The black spectrum is scaled to match the counts of the red spectrum in the region of interest between 11.0 MeV and 19.5 MeV. The region of interest for the ^{22}Ne$(p,\gamma)^{23}$Na is marked by two blue lines

4. Discussion

The strengths of the newly observed resonances were used as input for the calculation of the ^{22}Ne$(p,\gamma)^{23}$Na thermonuclear reaction rate. The input of the calculation is summarized in the last column of table 1.

To calculate the thermonuclear reaction rate a Monte Carlo sampling technique was used, assuming a Gaussian distribution for the resonance energy and a log-normal distribution for the resonance strength. Moreover, the probability density function of the tentative resonances at 71, 105 and 215 keV was built from the experimental data, extracting the number of counts in the region of interest from the Poisson distributions associated to the signal and the background respectively.

Figure 6 shows the results on the thermonuclear reaction rate. Low, median and high estimations of the rate were calculated at each temperature using 0.16, 0.50 and 0.84 quantiles for the probability density function of the total rate. In the calculation of the low rate, the strength of the resonances at 71, 105 and 215 keV was set to zero, while 1/10 of the upper limit value was used to obtain the median rate and the full upper limit value was used to obtain the high rate. The fractional contribution of the resonances which play a significant role in the total rate is reported in colors in figure 6. A more complete discussion of the astrophysical implications can be found in [5] and [29].

PoS(INPC2016)148

E_R	$\omega\gamma$ [eV]	
[keV]	LUNA HPGe [13, 5]	Adopted
29		$\leq 2.6 \times 10^{-25}$ [11]
37		$(3.1 \pm 1.2) \times 10^{-15}$ [11]
71	$\leq 1.5 \times 10^{-9}$	$\leq 1.5 \times 10^{-9}$
105	$\leq 7.6 \times 10^{-9}$	$\leq 7.6 \times 10^{-9}$
156.2	$(1.48 \pm 0.09_{stat} \pm 0.04_{syst}) \times 10^{-7}$	$(1.48 \pm 0.09_{stat} \pm 0.04_{syst}) \times 10^{-7}$
189.5	$(1.87 \pm 0.03_{stat} \pm 0.05_{syst}) \times 10^{-6}$	$(1.87 \pm 0.03_{stat} \pm 0.05_{syst}) \times 10^{-6}$
215	$\leq 2.8 \times 10^{-8}$	$\leq 2.8 \times 10^{-8}$
259.7	$(6.89 \pm 0.07_{stat} \pm 0.15_{syst}) \times 10^{-6}$	$(6.89 \pm 0.07_{stat} \pm 0.15_{syst}) \times 10^{-6}$
291		2.2×10^{-6} [8]
323		2.2×10^{-6} [8]
334		3.0×10^{-6} [8]
369		6.0×10^{-4} [14]
394		6.0×10^{-4} [14]
436		0.079 ± 0.006 [12]
479		0.594 ± 0.038 [12]
638.5		2.45 ± 0.18 [12]
661		0.032 ± 0.017 [12]

Table 1: Resonance strengths obtained after the HPGe phase and used in the calculation of the thermonuclear reaction rate. Upper limits by LUNA are given at 90% confidence level. For $E_R >$ 661 keV the strengths in [11] were adopted.

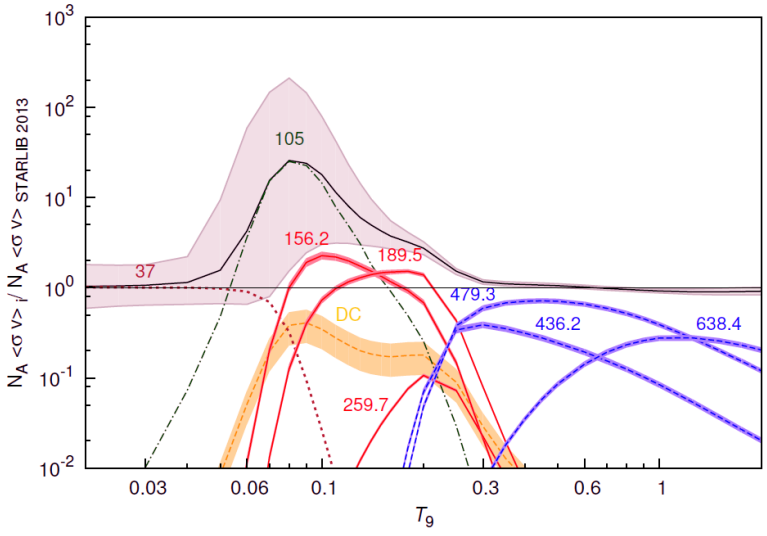

Figure 6: Thermonuclear reaction rate normalized to STARLIB 2013. A description of the figure is given in the text.

PoS(INPC2016)148

References

[1] E. Carretta *et al.*, *Na-O anticorrelation and HB. VII. The chemical composition of first and second-generation stars in 15 globular clusters from GIRAFFE spectra*, *Astron. Astrophys.*, **505** (2009) 117-138

[2] C. L. Doherty *et al.*, *Super and massive AGB stars - II. Nucleosynthesis and yields - Z = 0.02, 0.008 and 0.004*, *Monthly Notices Royal Astronom. Soc.*, **437** (2014) 195-214

[3] T. Decressin *et al.*, *Fast rotating massive stars and the origin of the abundance patterns in galactic globular clusters*, *Astron. Astrophys.*, **464** (2007) 1029-1044

[4] A. L. Sallaska *et al.*, *STARLIB: A Next-generation Reaction-rate Library for Nuclear Astrophysics*, *Astrophys. J. Suppl. Ser.*, **207** (2013) 18

[5] R. Depalo *et al.*, *Direct measurement of low-energy* ^{22}Ne$(p,\gamma)^{23}$Na *resonances*, *Phys. Rev. C*, **94** (2016) 055804

[6] R. G. Izzard *et al.*, *Reaction rate uncertainties and the operation of the NeNa and MgAl chains during HBB in intermediate-mass AGB stars*, *Astron. Astrophys.*, **466** (2007) 641-648

[7] J. Keinonen *et al.*, *Absolute resonance strengths in the* ^{20,21,22}*Ne(p,* γ*)*^{21,22,23}*Na and* ^{21}*Ne(p,* $p_1\gamma$*)*^{21}*Ne reactions*, *Phys. Rev. C*, **15** 579-586

[8] J. Görres *et al.*, *Search for low-energy resonances in* ^{21}*Ne(p,*γ*)*^{22}*Na and* ^{22}*Ne(p,*γ*)*^{23}*Na*, *Nucl. Phys. A*, **385** (1982) 57-75

[9] J. Görres *et al.*, *Proton-induced direct capture on* ^{21}*Ne and* ^{22}*Ne*, *Nucl. Phys. A*, **408** (1983) 372-396

[10] C. Iliadis *et al.*, *Charged-particle thermonuclear reaction rates: II. Tables and graphs of reaction rates and probability density functions*, *Nucl. Phys. A*, **841** (2010) 31-250

[11] C. Iliadis *et al.*, *Charged-particle thermonuclear reaction rates: III. Nuclear physics input*, *Nucl. Phys. A*, **841** (2010) 251-322

[12] R. Depalo *et al.*, *Strengths of the resonances at 436, 479, 639, 661, and 1279 keV in the* ^{22}*Ne(p,*γ*)*^{23}*Na reaction*, *Phys. Rev. C*, **92** (2015) 045807

[13] F. Cavanna *et al.*, *Three New Low-Energy Resonances in the* ^{22}*Ne (p ,*γ *)*^{23}*Na Reaction*, *Phys. Rev. Lett.*, **115** (2015) 252501

[14] S. E. Hale *et al.*, *Investigation of the* ^{22}*Ne(p,*γ*)*^{23}*Na reaction via (*^{3}*He,d) spectroscopy*, *Phys. Rev. C*, **65** (2001) 015801

[15] K. J. Kelly *et al.*, *New measurements of low-energy resonances in the* ^{22}**Ne**$(p,\gamma)^{23}$**Na** *reaction*, *Phys. Rev. C*, **95** (2017) 015806,

[16] A. Formicola *et al.*, *The LUNA II 400kV accelerator*, *Nucl. Inst. Meth. A*, **507** (2003) 609-616

[17] C. Broggini *et al.*, *LUNA: Nuclear Astrophysics Deep Underground*, *Annu. Rev. Nucl. Part. Sci.*, **60** (2010) 53-73,

[18] A. Caciolli *et al.*, *Revision of the* ^{15}*N(p,*γ*)*^{16}*O reaction rate and oxygen abundance in H-burning zones*, *Astron. Astrophys.*, **533** (2011) A66

[19] M. Marta *et al.*, *Nucl. Inst. Meth. A*, *Study of beam heating effect in a gas target through Rutherford scattering*, **569** (2006) 727-731

[20] F. Cavanna *et al.*, *A new study of the* ^{22}*Ne(p,* γ*)*^{23}*Na reaction deep underground: Feasibility, setup and first observation of the 186 keV resonance*, *Eur. Phys. J. A*, **50** (2014) 179

PoS(INPC2016)148

[21] A. Caciolli *et al.*, *Ultra-sensitive in-beam γ-ray spectroscopy for nuclear astrophysics at LUNA*, *Eur. Phys. J. A*, **39** (2009) 179-186

[22] D. Bemmerer *et al.*, *Feasibility of low-energy radiative-capture experiments at the LUNA underground accelerator facility*, *Eur. Phys. J. A*, **24** (2005) 313-319

[23] J. R. Powers *et al.*, *Nuclear Structure of ^{23}Na: The ^{22}Ne(^{3}He, d) Reaction*, *Phys. Rev. C*, **4** (1971) 2030-2046

[24] D. G. Jenkins *et al.*, *γ-ray spectroscopy of the A=23, T=1/2 nuclei ^{23}Na and ^{23}Mg: High-spin states, mirror symmetry, and applications to nuclear astrophysical reaction rates*, *Phys. Rev. C*, **87** (2013) 064301

[25] C. Angulo, *et al.*, *A compilation of charged-particle induced thermonuclear reaction rates*, *Nucl. Phys. A*, **656** (1999) 3-187

[26] H. Costantini *et al.*, *LUNA: a laboratory for underground nuclear astrophysics*, *Rep. Prog. Phys.*, **72** (2009) 086301

[27] G. Fiorentini *et al.*, *Prospects for underground accelerator research*, *Z. Phys. A*, **350** (1995) 289-301

[28] C. Casella *et al.*, *A new setup for the underground study of capture reactions*, *Nucl. Inst. Meth. A*, **489** (2002) 160-169

[29] A. Slemer *et al.*, *^{22}Ne and ^{23}Na ejecta from intermediate-mass stars: the impact of the new LUNA rate for ^{22}Ne(p, γ)^{23}Na*, *Monthly Notices of the Royal Astronomical Society*, **465** (2017) 4817-4837

PoS(INPC2016)148